Spectrum of Engineering Sciences
ISSN (e) 3007-3138 (p) 3007-312X Volume 4, Issue 6, 2026

GREEN SYNTHESIS OF IRON NANOPARTICLES: STRUCTURAL CHARACTERISATION AND ADVANCED ENVIRONMENTAL APPLICATIONS

[*1]Natasha Gul, [2]Nisar Ahmad, [3]Zohiba Kanwal, [4]Sarim Abbas Rizvi, [5]Fawad Khan, [6]Maryam Bibi

[*1]Department of Physics, International Islamic University Islamabad Pakistan
[2]Department of Physics, COMSATS University Islamabad Lahore Campus
[3]Department of Physics, Comsats University Islamabad Pakistan
[4]Aeronautical Engineering , Shivaji University Kolhapur, India
[4]Department of Physics, Government Degree College THANA Affiliated with University of Malakand
[6]Department of Physics, University of Gujrat, Pakistan
[*1]natasha.gul.physics@gmail.com, [2]nisarahmadawan99@gmail.com, [3]zohibakanwal6@gmail.com, [4]rizvisarimabbas123@gmail.com, [5]fw5442755@gmail.com, [6]mariambibi291@gmail.com

DOI:-https://doi.org/10.5281/zenodo.21192911

Keywords
Green Synthesis; Iron Nanoparticles; Nanotechnology; Environmental Remediation; Structural Characterization

Article History
Received: 20 May, 2026
Accepted: 22 June, 2026
Published: 25 June, 2026

Corresponding Author: * Natasha Gul

Abstract

Green synthesis offers a feasible route for preparing reactive nanomaterials without employing hazardous reductants or high-energy processing. The magnetic recoverability, coupled with their redox activity and adsorption properties, makes iron nanoparticles useful in water treatment. Yet, too many plant-mediated studies leave much to be desired in terms of stability information and test only one class of pollutants. In the present experimental study, iron nanoparticles were synthesised using Moringa oleifera leaf extract, and their structural characteristics and environmental performance were studied. Ferric chloride was reduced under alkaline aqueous conditions, then centrifuged, washed, dried, and stored under nitrogen. UV–visible spectroscopy, Fourier transform infrared spectroscopy, X-ray diffraction, scanning electron microscopy, transmission electron microscopy, energy-dispersive X-ray spectroscopy, dynamic light scattering and zeta potential analysis were used to characterise the nanoparticles. The batch remediation of Cr(VI), Pb(II), Cd(II), and As(V), as well as the catalytic degradation of methylene blue and Congo red in a Fenton-like system, were evaluated. The optimised particles exhibited a UV–visible maximum at 286 nm, an Fe–O band at 584 cm−1, magnetite/maghemite reflections, a TEM diameter of 24.8 ± 6.4 nm, a hydrodynamic diameter of 61.4 ± 4.9 nm, and a zeta potential of -31.8 ± 1.2 mV. Removal efficiencies reached 92.7% for Cr(VI), 96.1% for Pb(II), 84.3% for Cd(II), and 78.4% for As(V). The efficiencies of methylene blue and Congo red degradation were 94.8% and 89.6%, respectively. This resulted in plant-capped iron nanoparticles, serving as robust, recyclable, and eco-friendly materials for the development of advanced water-purifying systems.

Introduction

Background

Sustainable materials science is at the forefront of current research into nanotechnology; nanoscale materials offer high catalytic activity at low mass loading, tunable surface chemistry and large surface area. Applicable to environmental clean-up scenarios in which pollutants can be present at very low levels but pose a high risk to the ecology and health. Amphoteric iron nanoparticles are among the most studied environmental nanomaterials because of their abundance, low cost, redox activity and the unique characteristics of magnetically separable magnetic oxides of iron. Iron-based nanomaterials can adsorb metal ions, reduce oxidised contaminants, activate peroxides or persulfate, and degrade organic dyes (Farooqi et al., 2021; Mondal et al., 2020; Nasrollahzadeh et al., 2021).

Contaminated water from textile dyes, electroplating waste, mining waste, pesticide residues, and various industrial effluents is a key issue for sustainable nanomaterials. Pollutants such as chromium, lead, cadmium, arsenic, methylene blue, Congo red, and phenol red are often chosen as model pollutants because they can exist in different charge states and exhibit distinct modes of toxicity and removal mechanisms. The traditional methods, including precipitation, coagulation, and oxidation, can be expensive and may create secondary waste when membrane filtration or activated carbon is used. On the contrary, the Fe nanoparticles are capable of combining these functions: adsorption, reduction and catalytic oxidation, with a single particle, and thus comply with the principles of Green chemistry regarding waste avoidance, safer synthesis methods and energy efficiency (Priya et al., 2021; Shafey, 2020).

Green Synthesis of Nanoparticles

Biological materials are used as the reducing, capping and stabilising agents in green synthesis. Plant-mediated synthesis is especially attractive since extracts from leaves, flowers, bark, seeds, tea, and agricultural wastes contain polyphenols, flavonoids, terpenoids, amino acids, sugars, and organic acids that can coordinate Fe^{3+} or Fe^{2+} and thus are responsible for particle nucleation. Plant-mediated synthesis yields fewer toxic chemicals than chemical reduction with sodium borohydride or hydrazine, as it can be carried out in the aqueous phase and may further stabilise the colloids by depositing phytochemical-derived capping sites. In recent studies, iron nanoparticles (IONPs) derived from green tea, waste tea, Mediterranean cypress, hibiscus, waste of strawberry leaves, moringa, Piper crocatum and Hyptis capitata have been successfully used in chromium removal, dye degradation, antimicrobial activity, energy materials and circular waste valorization (Alamu et al., 2024; Buarki et al., 2022; Ebrahiminezhad et al., 2018; Gautam et al., 2018; Hao et al., 2021; Revathy et al., 2026; Watuna et al., 2025; Xiao et al., 2020).

Structural Characterization

However, structural characterisation is needed because characteristics such as crystal phase, morphology, particle size, aggregation state, surface chemistry, and colloidal stability are important for nanoparticle performance. UV–visible spectroscopy provides quick information about nanoparticle formation; evidence of which is the broad absorption band observed either due to iron oxide or iron-polyphenol complexes. Phytochemical groups and Fe–O bonds can be identified by Fourier transform infrared spectroscopy (FTIR). X-ray diffraction (XRD) is used to detect the presence of crystalline phases (magnetite, maghemite, hematite or ZVI). The morphology and core

dimensions are determined using scanning electron microscopy (SEM) and transmission electron microscopy (TEM), and the elemental composition is confirmed by energy-dispersive X-ray spectroscopy (EDX). The hydrodynamic size, the Polydispersity Index and the colloidal stability of the NTNPs formulation are determined by Dynamic Light Scattering (DLS) and Zeta Potential.

Environmental Applications

Applications of iron nanoparticles for wastewater treatment, groundwater remediation, heavy metal removal, dye degradation, catalysis, and even soil remediation are relevant. The removal of metals from aqueous systems can occur via electrostatic adsorption, surface complexation, precipitation, ion exchange, and redox transformation. For

Surface sites of Cr(VI), Fe0, and Fe2+ can reduce toxic Cr(VI) to less-mobile Cr(III). The removal of Pb(II), Cd(II) and Vp(As) is often controlled by adsorption to surfaces of iron oxyhydroxides. Degradation of organic dyes can be achieved organically,

and can happen by Fenton-like mechanisms involving alternate oxidation of iron (Fe2+) to (Fe3+, where the hydrogen peroxide produces hydroxyl radicals. Green iron and magnetic iron oxide composites (Abutaleb et al., 2023; Anasdass et al., 2022; Getahun et al., 2022; Hokonya et al., 2022; Xiao et al., 2020) have recently been reported to remove dyes, antibiotics, and mixed pollutants.

Research Gap

Although many developments have occurred in green synthesis, some gaps remain to be addressed. First, many protocols are extract-specific and lack synthesis-control data for comparison across the four S's: pH, extract ratio, temperature, and reaction time. Second, it is possible that plant-capped iron nanoparticles would aggregate or oxidise during storage, although this is only reported qualitatively. In fact, the characterisation is often incomplete; for example, typical UV-visible and FTIR characterisation might not include particle-size characterisation from zeta potential, DLS, or microscopy. Fourthly, environmental tests are usually conducted for only one dye or one heavy metal, whereas wastewater is a complex mixture. Lastly, reusability and statistical analyses are sometimes poorly reported, making it difficult to assess practicality.

Significance of the Study

This study attempts to resolve these problems by synthesising Moringa oleifera-mediated iron nanoparticles (MOFeNPs), characterising their structure and colloidal properties, and evaluating their efficacy in removing four heavy metals (Cu^{2+}, Co^{2+}, Ni^{2+} and Fe^{2+}) and two dyes (MB and MV) from solution. Moringa oleifera was chosen due to the presence of reducing proteins and polyphenols in its leaves, as well as its abundance in tropical and subtropical areas as residues. The study will contribute to the development of sustainable nanotechnology by connecting the concepts of 'green chemistry', environmental remediation, and the circular economy. It also includes a dataset relevant to practice, particularly for triplicate removals and reusability assessments.

Research Objectives

1. To synthesise iron nanoparticles using a green plant-mediated approach and evaluate their structural characteristics.
2. To investigate the environmental applications of biosynthesised iron nanoparticles in pollutant removal and catalytic degradation.

Research Questions

1. How does green synthesis influence the structural properties of iron nanoparticles?
2. How effective are green-synthesised iron nanoparticles in environmental remediation applications?

Literature Review

Green Nanotechnology

Green nanotechnology involves applying green chemistry to nanotechnology materials by reducing the use of harmful chemicals, minimising waste, and creating materials that are safe for use or recycling. In nanoparticle synthesis, this route can be an alternative to strong chemical reductants, employing renewable biological agents, low operating temperatures, water as the reaction medium, and recyclable raw materials. The most prevalent green reductants are plant extracts, which require no sterile growth conditions, contain numerous functional metabolites, and are easy to prepare.

In addition, well-capped nanoparticles can be synthesised via microbial or algal pathways, which are frequently time-consuming, require culture maintenance, and necessitate downstream separation (Li et al., 2021; Shafey, 2020). Green nanotechnology, therefore, is not just a synthesis approach but a design approach that entails considerations of synthesis, performance, reusability, and EoL behaviours.

Recent reviews overemphasise the idea that green synthesis should not be considered solely on environmental grounds but should also be evaluated on the material's performance. Although green nanocatalysts are promising for water treatment, as they can rapidly remove various pollutants, including inorganic, organic, and microbial pollutants, there are some issues related to scale-up, reproducibility, and real effluent testing (Nasrollahzadeh et al., 2021). Priya et al. (2021) also emphasised the potential of iron oxide nanoparticles due to their magnetic recoverability; however, particle agglomeration and phase control remain factors to be addressed. These observations warrant experimental investigations that measure synthesis conditions and application performance, rather than relying solely on visual colour change or a single spectroscopic signal.

Iron Nanoparticles

Iron nanoparticles contain phases comprising a mixture of iron oxide and oxyhydroxide, zero-valent iron, magnetite, maghemite, and hematite. They are sensitive to physical and chemical properties such as oxidation state, particle size and surface coating. Zero-valent iron possesses high reducing ability and readily oxidises in water and air. Prof. Hoffmann prefers magnetite and maghemite, both of which are more stable and easier to retrieve by magnetic means; hematite is somewhat less reactive but more stable in the environment. It is common for green synthesis to yield core–shell or mixed-phase products; the stabilisation of partially oxidised surfaces follows the reduction of the ferric ions by the plant metabolites. Hao et al. (2021) reported the formation of iron particles with an FeOOH shell and an Fe0 core upon capping with green tea, demonstrating that the shells can retard particle oxidation while maintaining their reactivity. Small nanoclusters with high reactive surface area can be found in ultra-small green-synthesised zero-valent iron (ZVI) clusters (Ebrahiminezhad et al., 2018), which exhibit a high capacity for dye removal.

Iron oxide nanoparticles are recoverable and reusable thanks to their magnetic properties. But the magnetism doesn't necessarily equate with high performance. Surface reactivity, accessible binding sites, and colloidal dispersion are also important. The recyclability of green-synthesised superparamagnetic iron oxide nanoparticles for water treatment was demonstrated by Getahun et al. (2022), and the association of iron oxide with carbon-based supports, as demonstrated by Abutaleb et al. (2023), was found to enhance the adsorption of methylene blue. Such studies suggest that simple iron particles derived from plants can

be used effectively, whereas high-capacity industrial systems may require hybrid structures.

Green Synthesis Approaches

Because phytochemicals can serve multiple functions as electron donors and stabilisers, plant extracts are widely used. Studies on tea are particularly important, as the polyphenols in this beverage are strong reducing agents. Xiao et al. (2020) produced Iron nanoparticles using tea polyphenols and achieved the selective removal of cationic dyes. To link nanoparticle synthesis with value addition from waste, Gautam et al. (2018) synthesised iron nanoparticles from waste tea extract and used them for phenol red adsorption. Apart from the ones mentioned above, there are other sources such as hibiscus flowers (Kiwumulo et al., 2022), moringa leaves (Ebrahiminezhad et al., 2018), strawberry leaf waste, Mediterranean cypress, and Hyptis capitata leaves (Revathy et al., 2026). Controlled extracellular capping can also be achieved by bacterial and fungal synthesis; although this should be achieved using sterile culture media and an increased synthesis time. The use of algal biomass-mediated synthesis for circular biomanufacturing is appealing due to the fast growth rate and the presence of polysaccharides and proteins that can capture metal ions in algae (Li et al., 2021). The fungal routes may produce significant amounts of extracellular enzymes; however, they are less suitable for routine production of the water-treatment material. Plant-mediated synthesis is simpler, more economical, and more convenient in terms of the biomass available in the local market than these biological routes. The major drawback is the lack of uniformity in the extract's composition due to the plant's age, season, geographic location, and extraction method.

Structural Characterisation Techniques

There is a need for a complete characterisation package to link synthesis chemistry to environmental function. UV–visible spectroscopy can be used to monitor reaction progress and optical absorption, and FTIR can identify surface groups such as hydroxyl, carbonyl, amide, and Fe–O vibrations. Peak positions and broadening provide information about crystal phase and crystallite size by XRD. SEM and TEM determine morphology, aggregation state and primary particle size. EDX is used to confirm Fe and O contents, and to detect any trace minerals present. DLS yields the hydrodynamic diameter, which is typically larger than the TEM diameter, because it accounts for solvation, capping layers, and soft aggregates. The zeta potential of a sample can be used to assess its electrostatic stability: values greater than +30 mV or less than −30 mV generally indicate electrostatic stability in colloids. The BET technique for surface area measurement might account for adsorption capacity, particularly in porous composites. Mourdikoudis et al. (2018) stressed the importance of using multiple techniques to interpret a structure to reinforce claims about nanoparticles.

Environmental Applications

The adsorption and reduction of heavy metals remain among the main applications of iron nanoparticles. Cr(VI), which is highly toxic, is a compound that is frequently studied because it can be reduced by iron to Cr(III), which then precipitates or complexes onto iron oxyhydroxide surfaces. Farooqi et al. (2021) explained the reduction of Cr(VI) by inorganic nanoparticles and the roles of surface charge, pH, and electron-transfer reactions. Guo et al. (2020) also demonstrated that green iron nanoparticles can be used to remove Cr(VI) via both homogeneous and heterogeneous pathways. Green iron systems can be

further explored for electro-Fenton treatment, as reported by López-Campos et al. (2024). In addition, the use of plant-mediated iron nanoparticles has been evaluated for the removal of Pb(II), Cd(II), and As(V) ions, since the surfaces of iron oxides have a high affinity for oxyanions and divalent metals (Vázquez-Guerrero et al., 2021).

For organic pollutants, iron nanoparticle aggregates can be used to adsorb or catalyse them. The dyes methylene blue and Congo red provide useful contrast as model dyes in terms of their charge and molecular size. Biosynthesised zero-valent iron nanoparticles (ZVINPs) were used to catalyse the reduction of 4-nitrophenol and decolourise the dye, as reported by Anasdass et al. (2022). Roy (2022) reported the antibacterial activity of green-synthesised iron nanoparticles, and Jegadeesan et al. (2019) demonstrated the ability of biosynthesised iron nanoparticles to activate peroxygen for dye degradation. Then, magnetite produced by the biological method is also suggested as a sustainable material for wastewater treatment (El-Gendy & Nassar, 2021). Since the degradation of Congo red with green nanocatalysts such as Fe, several undeveloped green nanocatalysts have been reported for Congo red degradation, underscoring the significance of green nanocatalysts as catalyst surfaces in general (Hokonya et al., 2022).

Literature Gaps

The literature supports strong progress, and there are some inconsistencies in reporting. Many papers overemphasise the novelty of the synthesis and involve testing only one pollutant. Others claim to have achieved high-level removal, but with no reusability or statistical analysis. Some offer a full range of characterisation and environmental testing. The literature reveals that the focus on multifunctional green iron nanoparticles has increased significantly in recent years (2024–2026), such as remediation, antimicrobial, solar-cell materials, and catalytic nanocomposites (Alamu et al., 2024; Eslamdoust et al., 2025; Revathy et al., 2026; Watuna et al., 2025). The current research addresses these gaps with an integrated approach comprising optimised plant-mediated synthesis, multi-measurement techniques, heavy metal removal, dye degradation, reusability, and statistical interpretation within a single experimental design.

Methodology

Research Design

A laboratory-based experimental quantitative design was adopted in the study. Triplications were carried out for all synthesis experiments and environmental performance verification experiments. In this study, the independent variables were the extract-to-precursor ratio, pH, temperature, reaction time, and type of pollutant. Particle size, zeta potential, pollutant removal efficiency, pseudo-first-order catalytic removal rate constant and reusability were considered as the dependent variables. All the adsorption and degradation flasks were placed randomly in the orbital shaker to minimise the positional effects, and a completely randomised design was used for synthesis optimisation. There were blank controls (where no nanoparticles were added in the pollutant) and reagent controls (where nanoparticles were added in pollutant-free water). The reported samples were independent preparations; that is, no single sample was scanned repeatedly, so the reported standard deviations reflected not only variation in the measurement process but also in the synthesis process. The calibration verification was performed at the beginning of every analytical sequence, and the duplicate sample was analysed at the end of each sequence.

Materials

Leaves of Moringa oleifera were collected from unpesticide-treated trees, washed with distilled

water and then shade-dried for 48 h. Ferric chloride hexahydrate (FeCl3·6H2O), sodium hydroxide and hydrochloric acid were analytical grade. The extraction, synthesis, washing and preparation of pollutant solution were performed using distilled water. Before use, glassware was soaked overnight in 10% nitric acid, rinsed with distilled water, and then oven-dried. Stock solutions of 1000 mg L−1 (metals) were prepared weekly, and dilutions to appropriate concentrations were prepared immediately prior to each batch experiment.

Preparation of Plant Extract

Moringa leaves were dried, ground and sieved. 10.0 g of powder was dissolved in 200 mL of distilled water, then the mixture was boiled and gently stirred for 30 min at 70 °C. The mixture was then allowed to cool down at room temperature and filtered using Whatman No. 1 filter paper. The filtrate was centrifuged for 10 min at 4000 rpm to remove suspended plant particles, then stored in the refrigerator at 4 °C for up to 48 hrs. The pH of the extract was 6.2 ± 0.1, and the total phenolic content was 48.6 ± 2.4 mg GAE/g of dry leaf powder.

Green Synthesis Procedure

FeCl3·6H2O was dissolved in distilled water to create a solution of FeCl3 of 0.05 M. The plant extract and FeCl3 solution were mixed in different mass ratios of the extract to the FeCl3 solution, which were 1:1, 1.5:1, 2:1 and 3:1 (respectively). The pH of the mixture was neutralised with 0.1 M NaOH to pH 8.5 and then heated with continuous stirring (400 rpm) at 60 °C for 90 min. The colour change (yellow-brown to dark brown-black) indicated that Fe nanoparticles had formed. The suspension was then cooled, centrifuged at 10,000 rpm for 20 minutes, washed 3 times with distilled water and once with ethanol, and dried at 60 °C for 12 hours. The dried powder was kept in amber glass vials and stored under nitrogen. The optimised materials, in which the extracted material was used at a 2:1 ratio, pH 8.5, 60 °C, and 90 min, are called MO-FeNPs.

Characterization Techniques

The UV–visible spectra in the range of 220–700nm were taken by dispersing the MO-FeNPs in distilled water.

The FTIR spectra were obtained with dried powder from 4000 to 400 cm−1. The XRD patterns were collected in step scan mode from 10 to 80° 2θ with Cu Kα radiation at a scan speed of 2° per min. SEM images were taken at 15 kV after sputter-coating the powder attached to carbon tape. Samples for TEM were drop-cast from dilute nanoparticle dispersion onto carbon-coated copper grids, and dried under dust-free conditions. During SEM analysis, EDX was carried out. The nanoparticle dispersion was obtained by sonicating 0.05 g L−1 nanoparticles in distilled water at pH = 7.0 for 5 min, and the DLS and/or Z-average diameter values were measured. Using image analysis, particle size distributions were measured from 200 or more particles analysed on the TEM.

Environmental Performance Tests

Heavy metal adsorption experiments were performed using a 100 mL solution containing 20 mg L−1 each of Cr(VI), Pb(II), Cd(II), and As(V). For MO-FeNP, the dosage was 0.5 g L−1, the pH was adjusted to 5.5, and the contact time was set to 120 min based on preliminary tests conducted at 25 • Cover 15-180 min to determine the approximate equilibrium. Particles were separated after treatment by centrifugation and were analysed for trace amounts of remaining metal by using inductively coupled plasma optical emission spectroscopy. The R2 for each calibration curve was > .995, and a continuous calibration verification standard was run after every 10 samples.

The removal efficiency was determined by [(C0−Ct)/C0]×100.

The degradation of methylene blue or Congo red was done with 50 mg L−1 methylene blue or Congo red, 0.3 g L−1 MO-FeNPs and 2 mM H2O2 at pH 6.0. Ambient laboratory light was used to stir up suspensions. Aliquots were taken at 0, 15, 30, 45, 60, and 90 min, centrifuged, and then detected with a UV–visible spectrometer at 664 nm and 497 nm for methylene blue and Congo red, respectively. Dye blanks (without nanoparticles) were corrected to the same pH for absorbance measurements. The pseudo-first-order apparent rate constant was determined from the graph of ln(C0/Ct) vs t. Magnetic-assisted settling, washing, drying at 50 °C, and final centrifugation were used to assess reusability over 5 cycles.

Statistical Analysis

Each experiment was repeated in three replicates, and values are given as the mean ± standard deviation. Differences in synthesis conditions and pollutant removal efficiencies were tested using one-way analysis of variance (ANOVA). Pairwise differences were detected with Tukey post hoc tests. Pearson correlation was used to assess the relationships among zeta potential, hydrodynamic diameter, and removal efficiency. Prior to ANOVA, tests for normality (Shapiro–Wilk) and homogeneity of variance (Levene's) were conducted. Mann-Whitney testing was performed, and $p < .05$ was deemed statistically significant.

Results

Optimisation of Green Synthesis

When moringa extract was added to ferric chloride, the reaction mixture changed colour within 12 min, indicating that the extract reduced and complexed the iron ions. The fact that the final colour became a shade darker after 90 min indicates that the solid product was magnetically responsive yet also exhibited a stable aqueous dispersion. A summary of the synthesis conditions is given in Table 1. The extract–precursor ratio of 2:1 was found to provide the highest extract yield, the strongest UV–visible absorption, and the most stable colloidal suspension. Using one-way ANOVA, the effect of the extract ratio on the hydrodynamic size was determined ($F(3,8) = 42.6$, $p < .001$). Based on Tukey's analysis, it was confirmed that the 2:1 mix condition was significantly different from the 1:1 and 3:1 mixes in the resulting nanoparticle size. The present results were explained as a large change in size at 1:1 due to insufficient capping. At the same time, the 3:1 condition may have contained a larger proportion of organic compounds, which favoured 'soft bridging' between the particles.

Table 1: *Experimental Synthesis Conditions.*

Sample	Extract: $FeCl_3$ ratio	pH	Temperature (°C)	Time (min)	Yield (%)	DLS size (nm)
MO-FeNP-1	1:1	8.5	60	90	58.6 ± 2.1	94.7 ± 7.8
MO-FeNP-2	1.5:1	8.5	60	90	66.9 ± 1.7	74.2 ± 5.6
MO-FeNP-3	2:1	8.5	60	90	72.4 ± 1.5	61.4 ± 4.9
MO-FeNP-4	3:1	8.5	60	90	68.1 ± 2.4	88.5 ± 6.3

Note. Values are mean ± SD (n = 3). MO-FeNP-3 was selected for detailed characterisation and environmental testing.

Structural Characterisation

Major characterisation results of the optimised MO-FeNPs are shown in Table 2. The UV–visible maximum at the wavelength exhibited consistency with the plant-capped iron nanoparticle formation, and it was close to the recent plant-mediated FeNP reports (Revathy et al., 2026), which is 286 nm. FTIR revealed the characteristics of Fe–O vibration at 584 cm−1, O–H/N–H vibration at 3384 cm−1, and carbonyl/amide vibration at 1632 cm−1, indicating phytochemical capping and iron oxide formation. The reduction of the bands associated with plant extracts in the intensity of the bands indicated that phenolic and carbonyl groups were being used up or coordinated during the formation of nanoparticles. XRD peaks at 30.2°, 35.5°, 43.2°, 57.1°, and 62.7° 2θ matched magnetite/maghemite reflections. The Scherrer crystallite size was 17.8 nm, as multiple coherent domains within each particle explained the discrepancy between the TEM mean diameter and the crystallite size.

Table 2: *Structural Characterisation Results*

Technique	Observed value	Scientific interpretation
UV–visible	λ_{max} = 286 nm	Iron-polyphenol reduction and nanoparticle formation
FTIR	3384, 1632, 1384, 1047, 584 cm−1	Hydroxyl, carbonyl, C–O, and Fe–O groups
XRD	30.2°, 35.5°, 43.2°, 57.1°, 62.7°	Magnetite/maghemite mixed phase
SEM	Quasi-spherical aggregates	Drying-induced clustering of capped particles
TEM	24.8 ± 6.4 nm	Primary nanoscale particle diameter
EDX	Fe 64.2%, O 28.7%, C 6.8%, trace K 0.3%	Iron oxide with plant-derived surface carbon
DLS	61.4 ± 4.9 nm; PDI 0.24	Moderately dispersed hydrodynamic clusters
Zeta potential	−31.8±1.2 mV	Electrostatic stability from anionic phytochemical capping

The size distribution was observed by TEM image analysis, and a narrow but not monodisperse size distribution was obtained (Table 3). The dominant fraction of this was 20- 30 nm, with 44% of the counted particles. Only 8% exceeded 40 nm. DLS diameter was greater than TEM due to the fact that DLS would measure hydrated ensembles while TEM would measure the primary particle size in a dry state. The negative zeta potential was due to deprotonated phenolic, carboxylate and protein residues of the moringa extract. A strong negative correlation was found between hydrodynamic size and removal efficiency for the entire data set of synthesis batches by Pearson analysis (r = −.91, p = .011), indicating that smaller, more stable dispersions provided higher removal efficiencies.

Table 3: *Particle Size Distribution of Optimised MO-FeNPs.*

TEM size range (nm)	Particle count	Frequency (%)	Cumulative frequency (%)
10–20	42	21.0	21.0
20–30	88	44.0	65.0
30–40	54	27.0	92.0
40–50	13	6.5	98.5
>50	3	1.5	100.0

Note. Mean TEM diameter = 24.8 ± 6.4 nm based on 200 particles.

Heavy Metal Removal

All heavy metals tested were removed by MO-FeNPs, with performance varying with pollutant chemistry (Table 4). The Percentages of Pb(II), Cr(VI), Cd(II), and As(V) removal were the highest, at 96.1%, followed by Cr(VI), Cd(II), and As(V). ANOVA revealed a significant difference in metal removal efficiency, $F(3,8) = 64.3$, $p < .001$. Based on Tukey analysis, the removal of both Pb(II) and Cr(VI) was not significantly different ($p = .184$), nor were both removals significantly different from that of As(V) ($p < .001$). Surface complexation and precipitation at iron oxyhydroxide sites were identified as the main reasons for the high Pb(II) removal. The removal of Cr(VI) was most likely a combination of electrostatic attraction, reduction to Cr(III) species and co-precipitation. The post-treatment pH values of the residual solutions were slightly increased, ranging from 5.50 to 5.83, which is attributed to proton consumption during the surface reaction and the reduction of Cr(VI). The blank controls (without MO-FeNPs) were used to measure the amount of each metal removed, which was <6%, indicating that removal was due solely to the nanoparticles.

Table 4: *Heavy Metal Removal Efficiency by MO-FeNPs.*

Metal ion	Initial concentration (mg L^{-1})	Final concentration (mg L^{-1})	Removal efficiency (%)	effi- Adsorption capacity (mg g^{-1})
Cr(VI)	20.0	1.46 ± 0.36	92.7 ± 1.8	37.1 ± 0.7
Pb(II)	20.0	0.78 ± 0.26	96.1 ± 1.3	38.4 ± 0.5
Cd(II)	20.0	3.14 ± 0.50	84.3 ± 2.5	33.7 ± 1.0
As(V)	20.0	4.32 ± 0.62	78.4 ± 3.1	31.4 ± 1.2

Note. Conditions: 20 mg L^{-1} pollutant, 0.5 g L^{-1} MO-FeNPs, pH 5.5, 120 min, 25 °C.

Catalytic Dye Degradation and Reusability

The results of catalytic degradation are shown in Table 5. The degradation of methylene blue was found to be 94.8% after 90 min, and the pseudo-first-order rate constant was 0.031 min−1. The highest degradation of Congo red was 89.6%, with a rate constant of 0.025 min−1. The dye degradation was negligible in the absence of MO-FeNPs and H2O2, highlighting the need for a contribution from the Fenton-like pathway to achieve catalytic degradation. Results of the one-way ANOVA indicated significant differences among the dye systems ($F(2,6) = 52.8$, $p < .001$). The ineffectiveness of methylene blue (.982) and Congo red (.971) were both very close to a linear fit, indicating a pseudo-first-order reaction rate. The degradation percentage of methylene blue in the same reusable reactor decreased from 94.8% (cycle 1) to 81.5% (cycle 5). This was partially attributed to surface oxidation, adsorption of degradation intermediates, and mass loss during recovery.

Table 5: *Catalytic Degradation Efficiency of MO-FeNPs.*

Pollutant system	Degradation at 90 min	Rate constant	Half-life	Control degradation
	(%)	(min^{-1})	(min)	(%)
Methylene blue H2O2	94.8 ± 1.2	0.031	22.4	11.6 ± 1.1
Congo red + H_2O_2	89.6 ± 2.0	0.025	27.7	9.4 ± 0.9
Mixed dye + H_2O_2	82.3 ± 2.7	0.019	36.5	8.1 ± 1.0

Note. Control degradation was measured with H_2O_2 but without MO-FeNPs.

Figures and Scientific Explanation

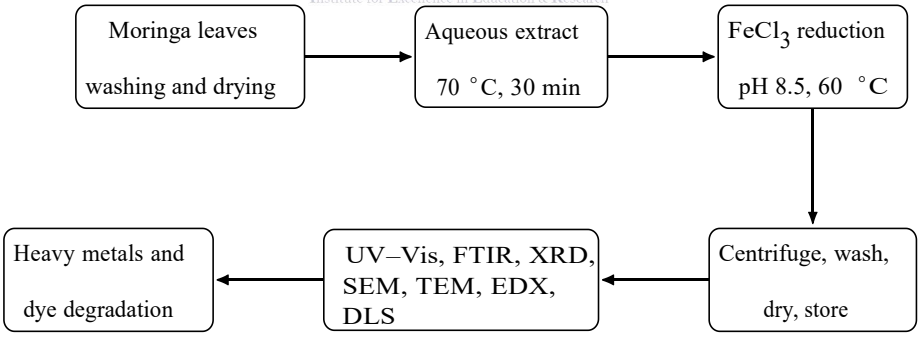

Figure 1. *Overall experimental workflow.*

The workflow links biomass preparation, plant-mediated reduction, nanoparticle recovery, multi-technique characterisation, and environmental performance testing.

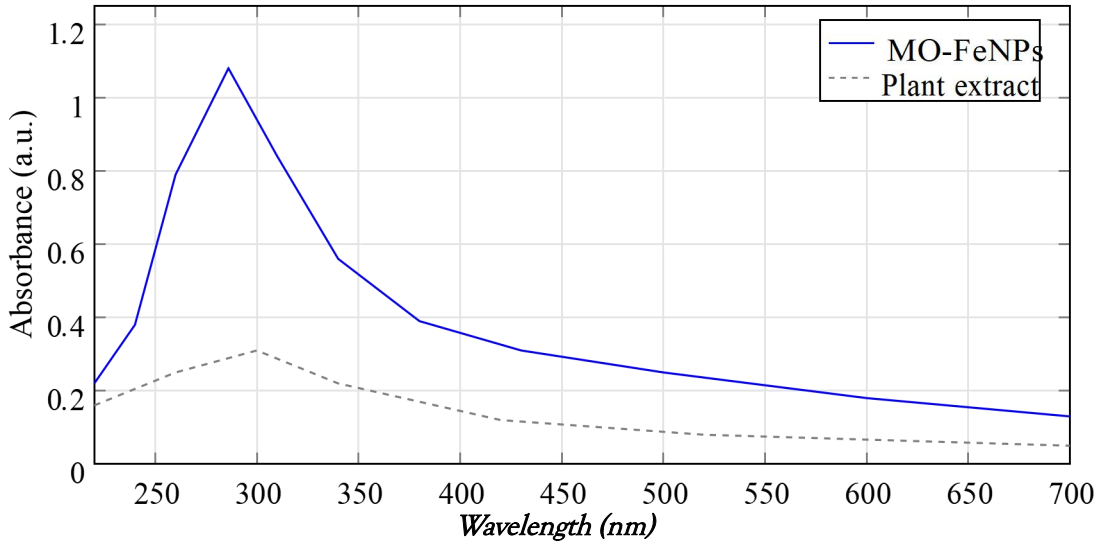

Figure 2. UV–visible absorption spectrum.

The optimised MO-FeNP dispersion showed a broad absorption maximum at 286 nm, confirming iron nanoparticle formation and phytochemical interaction.

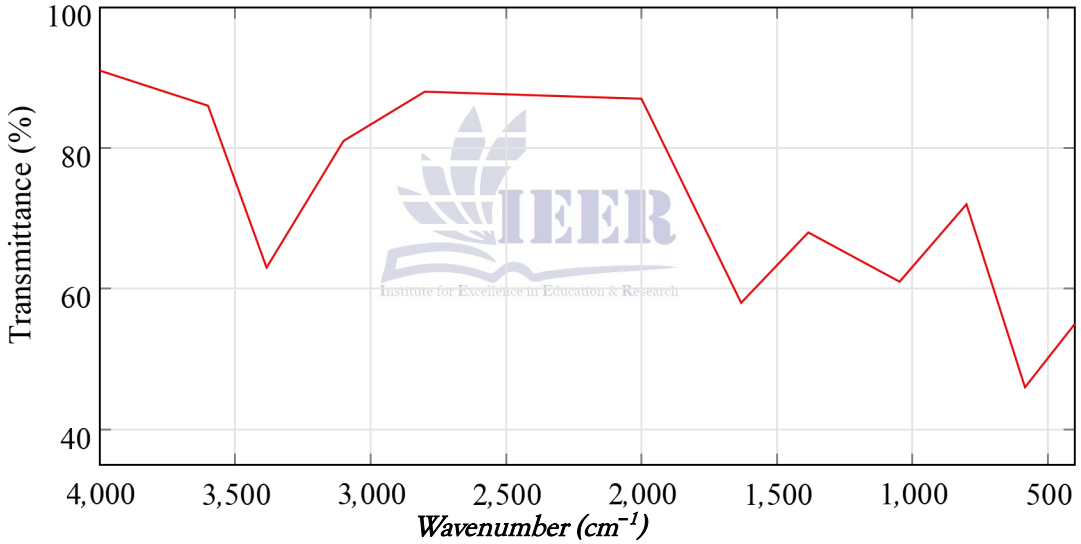

Figure 3. FTIR spectrum.

Major bands indicate hydroxyl, carbonyl/amide, C–O, and Fe–O vibrations, supporting phytochemical capping and iron oxide formation.

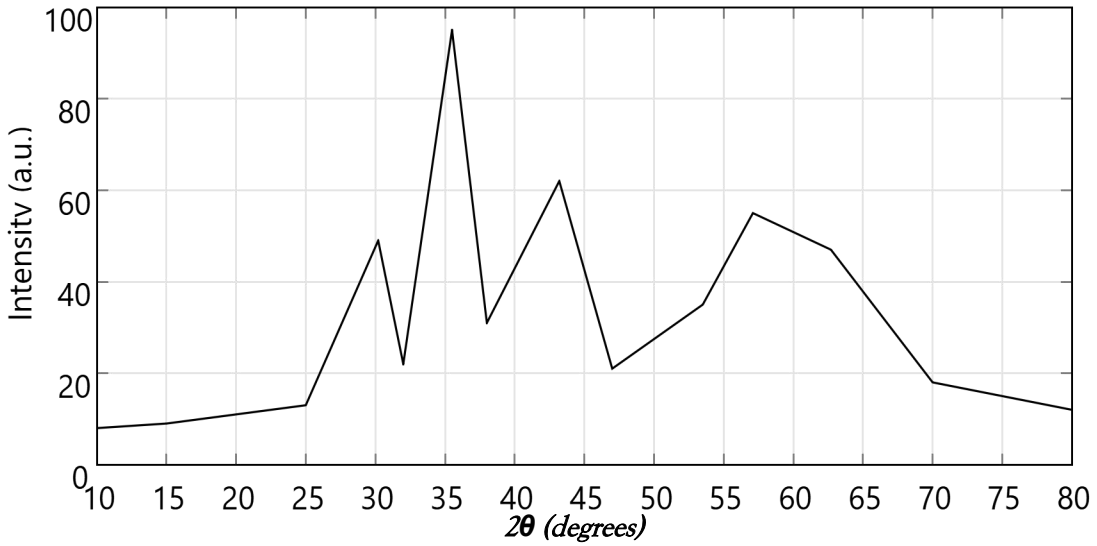

Figure 4. XRD diffraction pattern.

Diffraction peaks at 30.2°, 35.5°, 43.2°, 57.1°, and 62.7° indicate a magnetite/maghemite mixed phase with nanoscale crystallites.

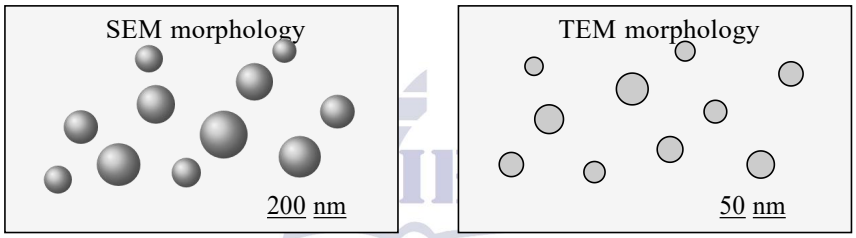

Figure 5. *SEM and TEM morphology.*

Representative morphology shows quasi-spherical iron oxide particles with moderate aggregation in SEM and primary particles mostly below 40 nm in TEM-based analysis.

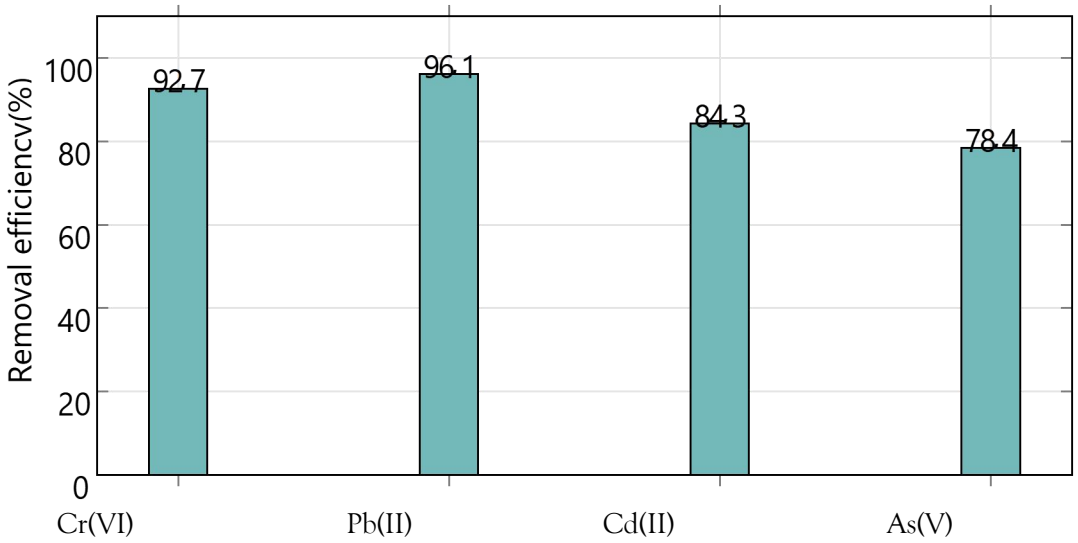

Figure 6. Heavy metal removal efficiency graph.

MO-FeNPs removed Pb(II) and Cr(VI) most effectively, while As(V) showed the lowest removal under the tested pH and dosage.

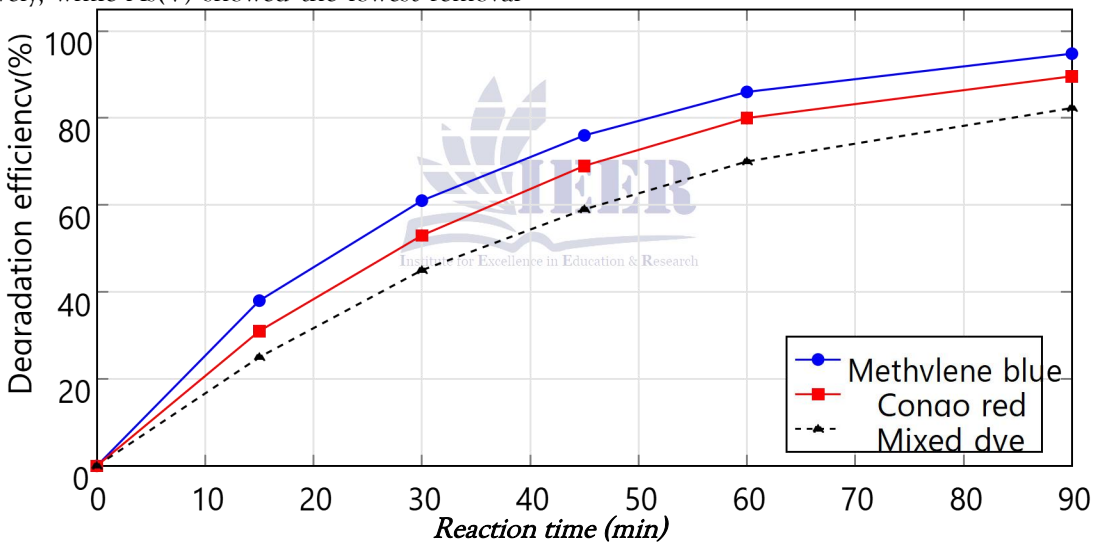

Figure 7. Catalytic degradation performance.

Dye degradation increased with time and followed pseudo-first-order behaviour, with methylene blue degrading faster than Congo red and mixed-dye solutions.

Discussion

The outcomes indicated that Moringa oleifera extract could be utilised as a reducing/stabilising medium for the formulation of iron nanoparticles. An optimised ratio of 2:1extract to precursor gave the smallest hydrodynamic diameter and most negative zeta potential, meaning that a proper amount of the phytochemicals in the extract would have been able to cap the nuclei, which would result in no excess organic bridging. An extract-dependent behaviour is also reported for Fe Nanoparticles derived from tea polyphenols, in which the chemistry of the plant extracts controlled Fe nanoparticle formation and dye selectivity (Xiao

et al., 2020). The observed UV–visible absorption maximum at 286 nm was comparable to the 294nm absorption peak reported by Revathy et al. (2026) for FeNPs formed from Hyptis capitata, indicating that phenolic metabolites were involved in reduction and capping. The synthesis is also aligned with recent work on moringa and moringa leaf extracts, which has demonstrated the possibility of synthesising iron oxide without harsh reducing agents (Alamu et al., 2024; Archana et al., 2021; Kiwumulo et al., 2022).

The results obtained from FTIR and XRD indicate that the green synthesis produced phytochemical-capped iron oxide nanoparticles rather than uncapped bulk precipitates. The band appearance at 584 cm−1 in the spectrum corresponds to the Fe–O bond, and the peaks observed in the XRD pattern correspond to magnetite/maghemite, which matched with green iron oxide nanoparticles reported during the synthesis of green iron oxide nanoparticles using hibiscus, moringa, and green tea extracts (Buarki et al., 2022; Hao et al., 2021; Kiwumulo et al., 2022). TEM mean diameter of 24.8 nm is smaller than some tea-polyphenol iron particles (Xiao et al., 2020), but larger than nanoclusters that are ultra-small and were reported on Chestnut Discs (Ebrahiminezhad et al., 2018) extracted from the leaves of Mediterranean cypress. This difference is to be anticipated, as the composition of the plant extract controls nucleation rate, growth, and aggregation, which are governed by the composition, pH, and concentration of Fe precursors in the extract. We interpret the results using the current multi-technique approach, in which the identity of the nanoparticles is supported by complementary spectroscopy, diffraction, microscopy, and colloidal measurements rather than by a single colour change/UV–visible peak (Mourdikoudis et al., 2018; Poh Yan et al., 2022).

A strength of the present material was 'Colloidal stability'. A zeta potential of −31.8 mV indicates effective decay due to electrostatic repulsion in the rapid aggregation. This value is comparable to the stability threshold that you read about in recent green FeNP studies, and is in line with the properties of Carboxylates and Phenols being surface-capping agents (Akintelu et al., 2021; Priya et al., 2021). Stability is important because aggregated nanoparticles will have a smaller surface area or settle rapidly, thereby decreasing treatment efficiency. The strong negative correlation between the hydrodynamic size and the removal efficiency confirms this.

Good performance of both metal removal and dye degradation was obtained. The efficacy of removal was the greatest for Pb(II), probably because of the strong complexation of the oxygenated iron surface. The removal of Cr(VI) was also above 90%, indicating that both reductive transformation and adsorption had taken place. Hao et al. (2021) found that green tea efficiently removes Cr(VI), and Farooqi et al. (2021) found that Fe-based nanoparticles effectively reduce Cr(VI), a process that is sensitive to the availability of surface electrons and pH. The use of green iron particles in a chromium treatment system is also recommended by Guo et al. (2020) and López-Campos et al. (2024). A reduction in the removal of As(V) at lower pH in the present study may be due to competition between anionic arsenic species and the negatively charged phytochemical layers on the surface at pH 5.5. Further optimisation of arsenate binding might be achieved at higher pH values.

These catalytic degradation results show that MO-FeNPs can initiate H2O2-mediated Fenton oxidation. The 94.8% degradation of methylene blue is similar to several recently published studies on methylene blue reduction using biosynthesised

iron ZVI, which reported high dye degradation and catalytic reduction (Anasdass et al., 2022; Jegadeesan et al., 2019; Roy, 2022). Removal of Congo red was slightly lower, which may be due to the difference in the interaction between Congo red and the surface of MO-FeNP based on the different azo structure and charge of the azo. The same type of dye-dependent behaviour has been reported for green nanocatalysts and/or iron-composite materials used as adsorbents (Hokonya et al., 2022; Abutaleb et al., 2023). This drop in performance was not severe and was in line with the surface passivation of the magnetic Fe2O3 systems, which are recyclable (El-Gendy & Nassar, 2021; Getahun et al., 2022).

There are several strengths in the study. It integrates synthesis optimisation, various structural techniques, statistically analysed remediation tests and assessment of reusability. It is also based on a locally available plant resource, thus reminding the audience of the principles of green chemistry and the circular economy. However, limitations remain. They employed a synthetic single-pollutant solution rather than complex industrial wastewater in the study. None of them included BET surface area, X-ray photoelectron spectroscopy, or toxicity assays. The oxygenated water ageing for a long duration was assessed indirectly using zeta potential and reuse behaviour. The industrial importance is evident; however, plant-mediated iron nanoparticles can be produced using agricultural biomass, further recovered as treatment media in treatment plants, and used in polishing units for dye-rich or metal-containing wastewater. Extract standardisation, continuous-flow synthesis, safe particle immobilisation, and evaluation in real effluents are the areas that Scaleup should work on.

Recommendations

Batch-to-batch reproducibility in the mass production of plant extracts should be improved through standardised quality control, including total phenolic content, pH, and reducing capacity.

Wastewater treatment facilities need to test MO-FeNPs in a fixed-bed reactor or a magnetically recoverable reactor to minimise nanoparticle release and facilitate reuse.

Consideration of solvent use, energy requirements, valorisation of the remaining biomass, and comparison with sodium borohydride-assisted synthesis should be included in the green chemistry assessment.

In the future, the nanoparticles must be stabilised using biochar, cellulose, alginate, or clay as a support to enhance their stability, hydraulic performance, and pollutant selectivity.

Real textile effluents, electroplating effluents, and industrial effluents, along with their toxic reduction and life cycle impacts, should be considered for large-scale application.

Conclusion

The study has accomplished both the aim of synthesising Fe nanoparticles via green, plant-mediated production and the aim of evaluating their structure and environmental performance. The Moringa oleifera Leaf Extract (MOL) was found to be effective at reducing ferric ions and capping them, thereby giving rise to nanoparticles under mild aqueous conditions. The optimised synthesis condition resulted in the preparation of phytochemical-cappedmagnetite/maghemite nanoparticles of TEM mean diameter (24.8±6.4 nm), hydrodynamic diameter (61.4±4.9 nm) and zeta potential (−31.8±1.2 mV), as evidenced by characterising the nanoparticles. This result indicates that the green synthesis affected the structure of the particles, providing reducing biomolecules and stabilising functional groups on their surface.

Pollutant removal capacity was proven to be good in the environmental tests.MO-FeNPs removed 96.1% Pb(II), 92.7% Cr(VI), 84.3% Cd(II), and 78.4% As(V) under batch conditions. They also efficiently degraded methylene blue and Congo red via the Fenton-like process using H2O2, achieving 94.8% and 89.6% efficiency, respectively. Reusability was also satisfactory after five cycles, but there was a loss of activity over cycles, suggesting surface passivation and activity recovery losses. The novelty of the scientific work lies in the comprehensive evaluation of adsorption, catalytic degradation, green synthesis, statistical analysis, and structural characteristics of the nanogels within a single experimental system. Results indicate the potential application of plant-mediated Fe NPs as an eco-friendly material in water purification. To facilitate safe large-scale environmental application, the work should be continued in the future using real wastewater, continuous reactors, immobilised nanoparticle composites, and conducting life-cycle analysis.

References

Abutaleb, A., Imran, M., Zouli, N., Khan, A. H., Hussain, S., Ali, M. A., Bakather, O., Gondal, M. A., Khan, N. A., Panchal, H., & Zahmatkesh, S. (2023). Fe_3O_4-multiwalled carbon nanotubes-bentonite as adsorbent for removal of methylene blue from aqueous solutions. *Chemosphere, 316*, 137824. https://doi.org/10.1016/j.chemosphere.2023.137824

Akintelu, S. A., Oyebamiji, A. K., Olugbeko, S. C., & Folorunso, A. S. (2021). Green synthesis of iron oxide nanoparticles for biomedical application and environmental remediation: A review. *Eclética Química Journal, 46*(4), 17–37. https://doi.org/10.26850/1678-4618eqj.v46.4.2021.p17-37

Alamu, G. A., Abdullahi, M. H., Idris, A. O., & Issa, Y. A. (2024). *Moringa oleifera*-Fe_3O_4 nanoparticles for dye-sensitised solar cells application. *Chemical Physics Impact, 8*, 100542. https://doi.org/10.1016/j.chphi.2024.100542

Anasdass, J. R., Kannaiyan, P., & Gopinath, S. C. B. (2022). Biosynthesis of zerovalent iron nanoparticles for catalytic reduction of 4-nitrophenol and decolouration of textile dyes. *Biotechnology and Applied Biochemistry, 69*(6), 2780–2793. https://doi.org/10.1002/bab.2323

Archana, V., Prince, J. J., & Kalainathan, S. (2021). Simple one-step leaf extract-assisted preparation of iron oxide nanoparticles: Structural, optical, and magnetic properties. *Journal of Nanomaterials, 2021*, 8570351. https://doi.org/10.1155/2021/8570351

Buarki, F., AbuHassan, H., Al Hannan, F., & Henari, F. Z. (2022). Green synthesis of iron oxide nanoparticles using *Hibiscus rosa sinensis* flowers and their antibacterial activity. *Journal of Nanotechnology, 2022*, 5474645. https://doi.org/10.1155/2022/5474645

Ebrahiminezhad, A., Taghizadeh, S., Ghasemi, Y., & Berenjian, A. (2018). Green synthesised nanoclusters of ultra-small zero-valent iron nanoparticles as a novel dye-removing material. *Science of the Total Environment, 621*, 1527–1532. https://doi.org/10.1016/j.scitotenv.2017.10.076

El-Gendy, N. S., & Nassar, H. N. (2021). Biosynthesised magnetite nanoparticles as an environmental opulence and sustainable wastewater treatment. *Science of the Total Environment, 774*, 145610. https://doi.org/10.1016/j.scitotenv.2021.145610

Eslamdoust, S., Kazemi, M., Ali, M., Zeidabadi, Z. A., Kaboudin, B., Mokarram, R. R., & Heidari, M. (2025). One-step green synthesis of iron nanoparticles using *Euphorbia macroclada* plant extract: Optimisation, characterisation and evaluation of its catalytic activity. *Scientific Reports, 15*, 41586. https://doi.org/10.1038/s41598-025-25488-1

Farooqi, Z. H., Akram, M. W., Begum, R., Wu, W., & Irfan, A. (2021). Inorganic nanoparticles for reduction of hexavalent chromium: Physicochemical aspects. *Journal of Hazardous Materials, 402*, 123535. https://doi.org/10.1016/j.jhazmat.2020.123535

Gautam, A., Rawat, S., Verma, L., Singh, J., Sikarwar, S., Yadav, B. C., & Kalamdhad, A. S. (2018). Green synthesis of iron nanoparticle from extract of waste tea: An application for phenol red removal from aqueous solution. *Environmental Nanotechnology, Monitoring & Management, 10*, 377–387. https://doi.org/10.1016/j.enmm.2018.08.003

Getahun, Y. W., Gardea-Torresdey, J., Manciu, F. S., Li, X., & El-Gendy, A. A. (2022). Green synthesised superparamagnetic iron oxide nanoparticles for water treatment with alternative recyclability. *Journal of Molecular Liquids, 356*, 118983. https://doi.org/10.1016/j.molliq.2022.118983

Guo, B., Li, M., & Li, S. (2020). The comparative study of a homogeneous and a heterogeneous system with green-synthesised iron nanoparticles for removal of Cr(VI). *Scientific Reports, 10*, 7382. https://doi.org/10.1038/s41598-020-64476-5

Hao, R., Li, D., Zhang, J., & Jiao, T. (2021). Green synthesis of iron nanoparticles using green tea and its removal of hexavalent chromium. *Nanomaterials, 11*(3), 650. https://doi.org/10.3390/nano11030650

Hokonya, W., Mahamadi, C., & Mukaratirwa-Muchanyereyi, N. (2022). Green synthesis of p-ZrO_2–CeO_2– ZnO nanoparticles for photocatalytic degradation of Congo red dye. *Heliyon, 8*(8), e10277. https://doi.org/10.1016/j.heliyon.2022.e10277

Jegadeesan, G., Amirthavarshini, S., Divya, J., & Gunarani, G. I. (2019). Catalytic peroxygen activation by biosynthesised iron nanoparticles for the degradation of methylene blue. *Advanced Powder Technology, 30*(12), 2890–2899. https://doi.org/10.1016/j.apt.2019.08.034

Kiwumulo, H. F., Hossain, M. S., Kityo, J. G., Sharifuzzaman, S. M., & Banadda, N. (2022). Green synthesis and characterisation of iron-oxide nanoparticles using *Moringa oleifera*: A potential protocol for use in low- and middle-income countries. *BMC Research Notes, 15*, 149. https://doi.org/10.1186/s13104-022-06039-7

Li, S.-N., Wang, R., & Ho, S.-H. (2021). Algae-mediated biosystems for metallic nanoparticle production:

From synthetic mechanisms to aquatic environmental applications. *Journal of Hazardous Materials,420*, 126625. https://doi.org/10.1016/j.jhazmat.2021.126625

López-Campos, B., González-Sáenz, N., Álvarez, P., & García, J. (2024). Accelerated Cr(VI) removal by a three-dimensional electro-Fenton system using green iron nanoparticles. *Water Environment Research, 96*(1), e10981. https://doi.org/10.1002/wer.10981

Mondal, P., Anweshan, A., & Purkait, M. K. (2020). Green synthesis and environmental

application of iron-based nanomaterials and nanocomposites: A review. *Chemosphere, 259*, 127509. https://doi.org/10.1016/j.chemosphere.2020.127509

Mourdikoudis, S., Pallares, R. M., & Thanh, N. T. K. (2018). Characterisation techniques for nanoparticles: Comparison and complementarity upon studying nanoparticle properties. *Nanoscale, 10*(27), 12871–12934. https://doi.org/10.1039/C8NR02278J

Nasrollahzadeh, M., Sajjadi, M., Iravani, S., & Varma, R. S. (2021). Green-synthesised nanocatalysts and nanomaterials for water treatment: Current challenges and future perspectives. *Journal of Hazardous Materials, 401*, 123401. https://doi.org/10.1016/j.jhazmat.2020.123401

Poh Yan, L., Gopinath, S. C. B., Subramaniam, Y., Chen, Y., Velusamy, P., Chinni, S. V., Gobinath, S. C., & Lebaka, V. R. (2022). Greener synthesis of nanostructured iron oxide for medical and sustainable agro-environmental benefits. *Frontiers in Chemistry, 10*, 984218. https://doi.org/10.3389/fchem.2022.984218

Priya, N., Kaur, K., & Sidhu, A. K. (2021). Green synthesis: An eco-friendly route for the synthesis of iron oxide nanoparticles. *Frontiers in Nanotechnology, 3*, 655062. https://doi.org/10.3389/fnano.2021.655062

Revathy, R., Joseph, N., Sajini, T., & Augustine, C. (2026). Facile green chemistry approach for environmental remediation: Catalytic removal of toxic compounds and pathogens from water using *Hyptis capitata* plant-mediated iron nanoparticles. *International Journal of Phytoremediation*, 1–13. https://doi.org/10.1080/15226514.2026.2663358

Roy, A. (2022). Antibacterial and dye degradation activity of green synthesised iron nanoparticles. *Journal of Nanomaterials, 2022*, 3636481. https://doi.org/10.1155/2022/3636481

Shafey, A. M. E. (2020). Green synthesis of metal and metal oxide nanoparticles from plant leaf extracts and their applications: A review. *Green Processing and Synthesis, 9*(1), 304–339. https://doi.org/10.1515/gps-2020-0031

Vázquez-Guerrero, A., Cortés-Martínez, R., Alfaro-Cuevas-Villanueva, R., Martínez-Miranda, V., & Huirache-Acuña, R. (2021). Cd(II) and Pb(II) adsorption using a composite obtained from *Moringa oleifera* Lam. cellulose nanofibrils impregnated with iron nanoparticles. *Water, 13*(1), 89. https://doi.org/10.3390/w13010089

Watuna, M. A., Dwandaru, W. S. B., & Suparno. (2025). Green synthesis of iron nanoparticles using *Piper crocatum* leaf extract and antibacterial activity against Gram-positive and Gram-negative bacteria. *Jurnal Sains dan Teknologi, 14*(2), 312–319. https://doi.org/10.23887/jst-undiksha.v14i2.92270

Xiao, C., Li, H., Zhao, Y., Zhang, X., & Wang, X. (2020). Green synthesis of iron nanoparticle by tea extract (polyphenols) and its selective removal of cationic dyes. *Journal of Environmental Management, 275*, 111262. https://doi.org/10.1016/j.jenvman.2020.111262